SEPERATION OF CO2 FROM NITROGEN AND OXYGEN USING HYDROPHOBIC CERAMIC MEMBRANE

Idris Abdullahi Hashim * , Habiba Shehu , Mamdud Hossain , Muktar Ramalan , Aditiya Karnik , Ayo Giwa

Posted Date: 18 October 2023

doi: 10.20944/preprints202310.1113.v1

Keywords: inorganic ceramic membrane; carbon capture; carbon emission; contact angle measurement; FTIR analysis; SEM analysis; gas separation

Article

Seperation of co2 from Nitrogen and Oxygen Using Hydrophobic Ceramic Membrane

Idris Abdullahi Hashim, Habiba Shehu, Mamdud Hossain, Ayo Giwa, James Njuguna, Aditiya Karnik and Muktar Ramalan

* Correspondence: i.hashim@rgu.ac.uk

Abstract: membrane separation technology shows promise, particularly gas separation membranes, including ceramic membrane. Ceramic membranes are increasingly gaining attention for their acid and alkali stability, corrosion resistance, high-temperature tolerance, and mechanical strength. This study focuses on alumina support ceramic membrane for CO_2 capture. The membranes were characterized using contact angle measurements, scanning electron microscopy (SEM), and Fourier Transform Infrared spectroscopy (FTIR) analysis. The contact angle measurements confirmed the hydrophilic, while SEM analysis showed even particle distribution in the alumina ceramic membranes respectively. EDAX analysis revealed the elemental composition in the alumina support matrix. FTIR analysis demonstrated chemical interactions of the support membrane. Single gas permeation experiments were conducted. It can be observed that Nitrogen gas permeated faster with increase in feed pressure through the unmodified ceramic inorganic hydrophobic membrane more than the other two single gases, O_2, and CO_2). As a result, only high permeance separation membranes with realistic size and pressure conditions may be considered of as a practical alternative for CO_2 capture. However, the presence of non-selective defects limited the improvement in selectivity of hydrophilic ceramic membrane. In this case, there is need to modify the ceramic membrane used to increase the flux, permeance of CO_2, and selectivity of CO_2.

Keywords: inorganic ceramic membrane; carbon capture; carbon emission; contact angle measurement; FTIR analysis; SEM analysis; gas separation

1. Introduction

Global temperatures are expected to rise by 2 to 4 degrees Celsius over the next century, according to projections. At latitudes further from the equator, polar amplification of warming is expected, resulting in more significant annual mean warming. This phenomenon is caused in part by melting snow, which absorbs more sunlight and reduces reflection into space in polar locations, boosting land surface heating. The equator, on the other hand, is anticipated to warm by less than 1°C, whereas 80°N or S latitude might warm by 3°C or more [1] Winter warming is expected to surpass summer warming at high latitudes due to comparable factors, but arid and semiarid places prone to summer drying will see more substantial warming during the summer.

According to predictions, sea levels will rise at a pace of about 1.8 cm per year due to melting ice caps and thermal expansion of saltwater caused by global warming. Even though we are still in the early stages of the expected global temperature rise caused by carbon dioxide emissions, scientists are confident in identifying a temperature increase during the last 150 years [5].

As a result, implementing measures to minimise CO_2 emissions is critical [6]. Prioritising energy-saving planning and techniques for reducing future emissions is critical for improving CO_2 emission reduction efforts [7].

Given the limits of traditional techniques, membrane engineering has emerged as a possible option. Notably, membrane-based CO_2 capture technologies offer a substantial benefit by reducing the requirement for high energy input during the extraction of CO_2 from sorbents, a contrast to standard sorbent-based [8]. The membrane system can function indefinitely, using less energy for separation or purification, and it has adaptable scalability for a wide range of applications [2,9]. Furthermore, as compared to chemical absorption, membrane separation technology enhances mass

 doi:10.20944/preprints202310.1113.v1

transfer by expanding the gas-liquid contact area, producing higher capture performance, reducing equipment size, and cutting desorption costs. The membrane separation method's flexibility allows for independent control of the gas-liquid flow rate, avoiding solvent loss, channels, bubbles, entrapment, and other operational difficulties. This method has a wide range of technological applications.

The introduction of ceramic membranes in the early 1960s constituted an important milestone in gas separation filtration, utilising porous ceramic materials for this purpose [3]. Ceramic membranes are divided into two types: porous ceramic membranes and dense ceramic membranes. Porous ceramic membranes have piqued the curiosity of researchers, notably for use in gas separation and as support materials. esearchers in the field of CO_2 capture are becoming more interested in membrane contactors due to their advantages in terms of offering a clear and stable phase interface, small size, a wide cross-sectional area, and simple linear scalability [1,6]. Ceramic membranes are frequently used in separation and purification processes because they outperform polymeric membranes in terms of structural, thermal, physical, and chemical durability [12,13].

2. Materials and Methods

The following is a list of the chemicals, materials, and gases used in the experiments described in this chapter:

Gases from BOC, UK (oxygen, Nitrogen, and carbon dioxide).

3. Equipment and instruments

1. Magnetic Stirrer by Fisher Scientific
2. Quantachrome instruments' automatic gas sorption analyzer

Fisher Scientific Beakers 3.

4. Weighing Balance Sartorius

Clifton Electric Water Bath No. 5

pH metre Checker's

Graphite Seals from Gee Graphite (Figure 8a)

Oxford Instruments SEM Scanning Electron Microscope

Zeiss Instruments' Energy Dispersive X-Ray Detector

Scientific Céramiques Techniques et Industriels (SCT), France, manufactures an alumina support membrane.

11. Thermocouple RS

Weir 413D Rotatory Dryer

Digitron Barnstead Electrothermal Power Regulator Temperature Gauge

14 Hand Tools (Spanners and Screwdrivers)

15. Omega Pressure Gauge

Roxspur Flow Metre No. 16

4. Methodology

4.1. Characterization hydrophobic ceramic membrane

4.4.1. SEM and EDAX Methodology

A Zeiss Evo LS10 S scanning electron microscope and an Oxford Instruments INCA System Energy Dispersive X-Ray analyser were used for SEM and EDAX studies, respectively. A coating of MgO powder was placed onto the adhesive side of the sample stub to prepare the samples. To reduce charging effects, the produced sample stub was coated with a silver solution, allowed to dry for 24 hours, and then a thin gold coating was placed on all samples. A working distance of 8.5 mm was used to collect SEM and EDAX pictures.

Preprints (www.preprints.org) | NOT PEER-REVIEWED | Posted: 18 October 2023 doi:10.20944/preprints202310.1113.v1

4.4.2. Methods: the FTIR Analysis

The functional groups in the synthesised MgO membrane were examined using an ATR Nicolet IS10 FT-IR spectrometer in the 400-4000 cm^{-1} spectral region.

4.4.3. Measurements of the contact angle

The Attention Theta Lite contact angle measuring equipment was used for the contact angle investigations. Using the sessile drop method, model liquids were dropped onto the pelleted materials to test wettability. A model liquid (water) was used to determine static contact angles. DIM was roughly 5.5 for ceramic membranes with pore widths of around 6000nm, and the average volume of water droplets upon initial contact with the solid surface served as the model liquid's average droplet volume.

The computer connected "One Attention" software programme was used to study and record the contact angles created by a single droplet of the model liquid. The picture captured were timed for various seconds at various frames per second (FPS). The ceramic membrane picture record was 240 seconds at 50% FPS. The computer calculated the angles arising from the model liquid droplet's right and left contact sites with the solid surface, as well as the baseline value. The programme then calculated the final average contact angle by averaging the angle data from the right and left positions (see Figure 1 and 2).

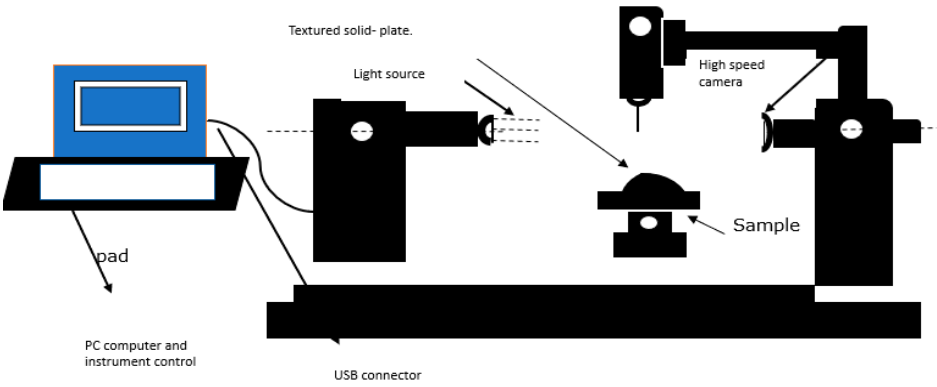

Figure 1. showing a schematic diagram of contact angle measurement set up.

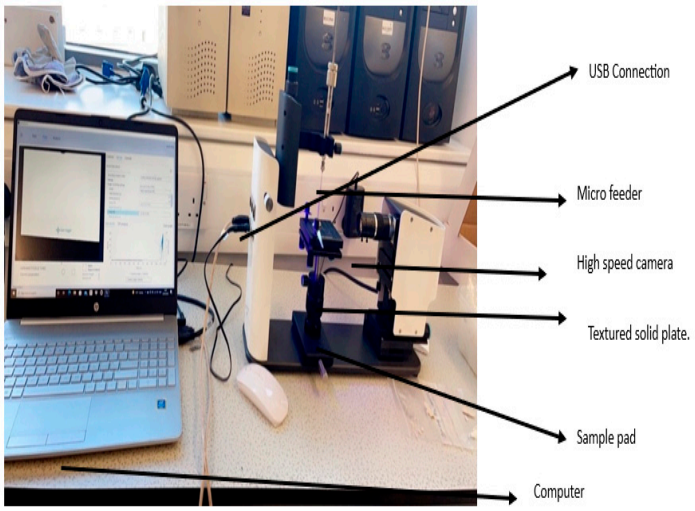

Figure 2. showing a diagram of contact angle measurement set up.

Preprints (www.preprints.org) | NOT PEER-REVIEWED | Posted: 18 October 2023 doi:10.20944/preprints202310.1113.v1

5. Gas Permeation Testing

The hydrophilic ceramic membrane was modified for direct air carbon capture by immersing a membrane support in a MgO-based solution and repeating dip coating techniques (three dips) with intervals of so-called gel procedures. To prevent gas leakage while improving data accuracy, a 6000-nm-pore size nanostructured commercial hydrophilic ceramic membrane with an effective permeable length of 32.8 cm, an outer diameter of 2.62 cm, an inner diameter of 1.96cm, and a permeance membrane surface area of 107.1cm was placed in a membrane reactor with a graphite ring as a seal. The retentate valves were kept closed, and the hydrophobic membrane was enclosed in a stainless-steel reactor. The schematic setup utilised to detect gas penetration is shown in Figure 3. T

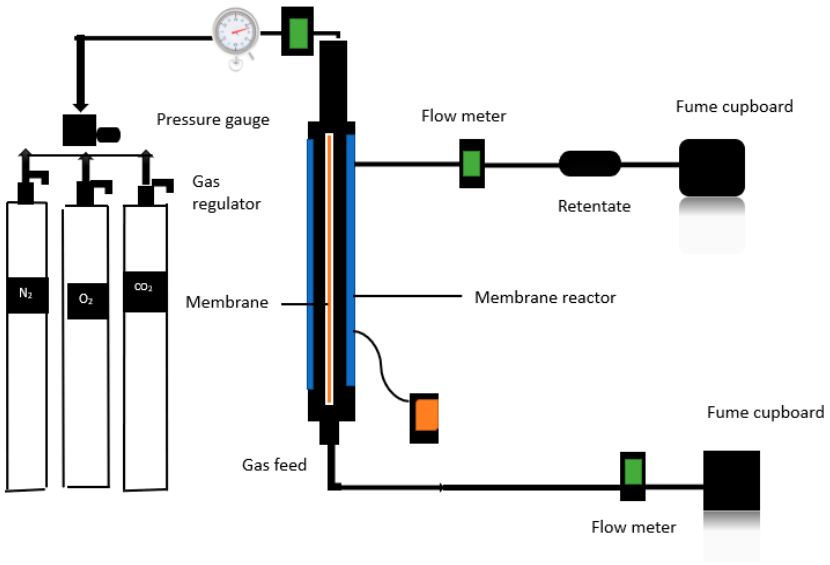

Figure 3. shows a schematic diagram of the experimental setup.

This includes a feed gas supply system and a pressure gauge that monitors reactor pressure. A valve regulates the supplied gas to control the flow. Gas permeations have been performed at temperatures ranging at 20 °C. To monitor the flow rate of the gas at a standard litre per minute (SLMP), a digital flow metre was mounted downstream of the permeate exit to the membrane reactor and after the pressure gauge.

Table 1. Summary of the Hydrophobic ceramic membrane parameters.

Hydrophilic ceramic membrane	Outer diameter (cm)	Inner diameter (cm)	Radius (cm)	Thickness (cm)	Permeance length (cm)	Wight (g)	Surface membrane area (cm^3)
6000nm (3mm)	1.04	0.77	0.52	0.27	32.8	48.9	107.1

6. Results and Discussions

6.1. Hydrophobic ceramic membrane characterization

6.1.1. SEM Analysis Findings

Figure 4 shows SEM pictures of the outer surface morphologies of the hydrophobic ceramic membrane at various magnifications. The particles are evenly distributed throughout the entire surface of the hydrophobic ceramic membrane. Notably, the hydrophobic ceramic membrane has a smooth and faultless surface with no fractures. The particle size of the sample, and its uniformity is visible throughout the membrane.

Preprints (www.preprints.org) | NOT PEER-REVIEWED | Posted: 18 October 2023 doi:10.20944/preprints202310.1113.v1

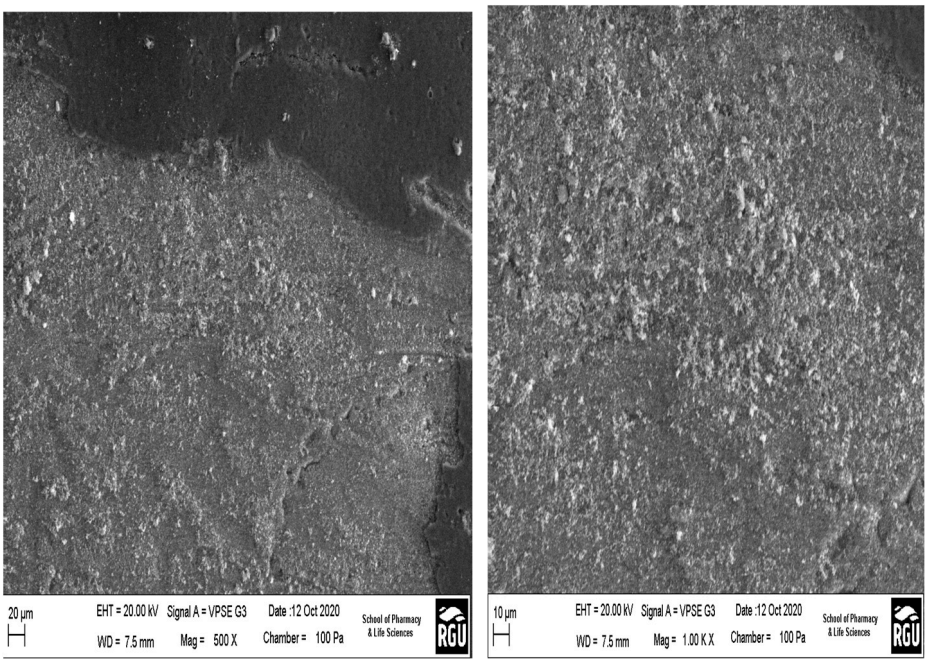

Figure 4. showing SEM's hydrophobic ceramic membrane.

6.1.2. Results of EDAX

Energy Dispersive X-ray Analysis (EDAX) was used to determine the elemental compositions of the alumina support and silica membrane. Figure 5 and Table 2 show the results in a sequential manner.

Spectrum analysis:
There were no missed peaks.
Spectrum processing:
No peaks omitted.
Processing option: All elements analysed.
Number of iterations = 4
Standard:
C $CaCO_3$
O SiO_2
Al Al_2O_3
Ti Ti

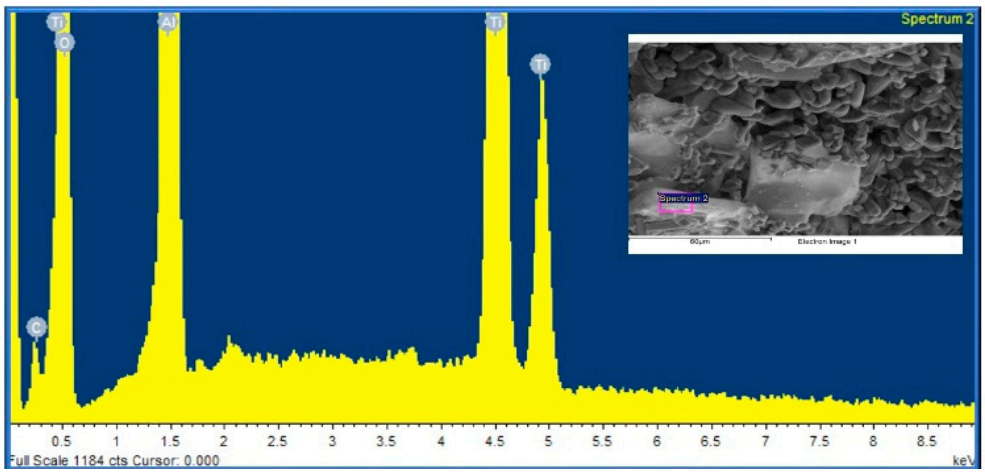

Figure 5. FTIR analysis of support hydrophobic ceramic membrane.

Preprints (www.preprints.org) | NOT PEER-REVIEWED | Posted: 18 October 2023 doi:10.20944/preprints202310.1113.v1

Table 2: Elemental composition of ceramic membrane.

Element	Weight%	Atomic%
C K	3.89	7.63
O K	40.10	58.96
Al K	24.53	21.39
Ti K	24.47	12.02
Totals	93.00	

6.1.3. FTIR analysis results

Figure 6 depicts the FTIR spectrum of the alumina support. The spectra show three distinct bands. The presence of C=O functional groups is seen in the band at 3323.4 cm^{-1}, whereas the presence of C-H functional groups is visible in the band at 3279.6 cm^{-1}. These findings are most likely due to the presence of aluminium oxide in the support.

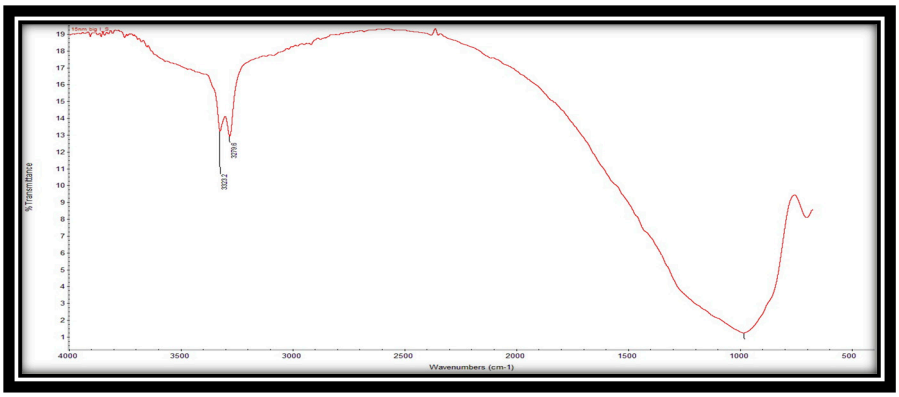

Figure 6. FTIR analysis.

6.1.4. Effect of wettability and surface-free energy on ceramic membranes for carbon capture

In the case of the support ceramic membrane, the initial contact angle value was measured at 108 degrees immediately after the first droplet was deposited on the surface, at 0 seconds (see Figure 7A). As time progressed, there was a slight reduction in the contact angle values as the droplet interacted with the ceramic membrane's surface. For instance, around 240 seconds (approximately towards the end of the interaction), the average contact angle values decreased to 94 degrees (see Figure 7B). This observation indicates an occurrence of adsorption, suggesting that interactions were taking place. At the approximate conclusion of the interaction, the contact angles had further decreased. Based on these outcomes, it can be deduced that the ceramic membranes used possess hydrophobic properties. The experimental contact angle results, employed as a characterization technique, validated the distinctions in the surface's physicochemical attributes.

Preprints (www.preprints.org) | NOT PEER-REVIEWED | Posted: 18 October 2023 doi:10.20944/preprints202310.1113.v1

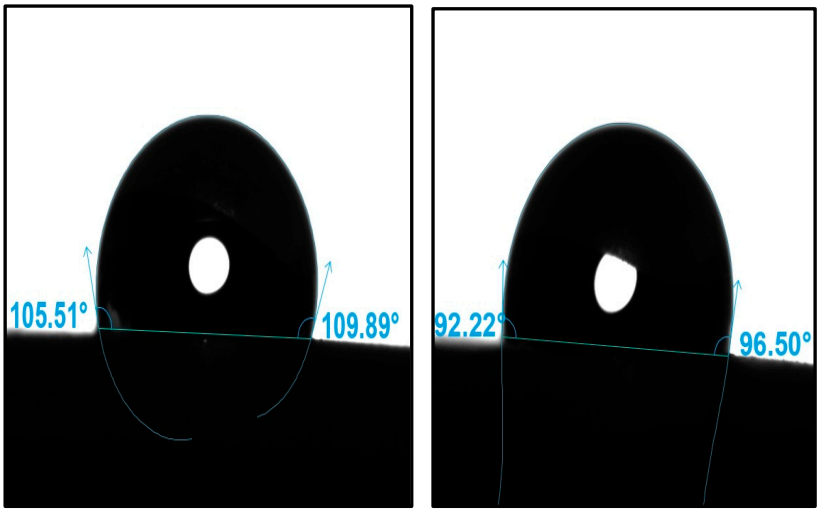

A. at 0 second *B at 240 second*

Figure 7. showing support ceramic membrane contact angle measurement's results.

Contact angle experiments are widely employed to assess surface energy, commonly using liquids like water. This technique measures the angle at which the liquid droplet on the surface forms. Determining the surface free energy (SFE) of a solid surface offers substantial insights into the interactions between various liquids and the employed ceramic membranes. The surface free energy outcomes, as obtained through contact angle measurements and presented in Table 3, yielded a value of 18.71 for the sample. Interpretation of these results suggests that the ceramic membrane's surface free energy indicates relatively lower interactions with water. This outcome indicates a low surface free energy for the sample, signifying limited interaction with the liquid.

The hydrophobic ceramic membrane, which is part of the support, exhibited less interaction with the liquid due to its inherent characteristics.

Table 3. shows the surface free energies of the samples used.

Method Equation of state	γ^{tot} [mN/m]	γ^{d} [mN/m]	γ^{p} [mN/m]
First MgO coated ceramic membrane	18.71	18.71	

7. Results and discussion

7.1. Gas permeation experimental results

7.1.1. Effect of pressure dependence of CO_2, N_2, O_2, gas fluxes

Gas flux across the ceramic membrane has a distinguishing characteristic (see Figure 8) This was accomplished by determining the flux J (mol m^{-2} s-1); the governing equation is as follows:

$$Flux\ J = \frac{flow\ rate\ [\frac{mol}{sec}}{membrane\ surface\ (m^2)} \quad (1)$$

where J is the gas flux over the membrane and mol. $s^{-1}m^{-2}$ is the ratio of the gas flow rate to the membrane surface area, which was determined to be 111.3.

Preprints (www.preprints.org) | NOT PEER-REVIEWED | Posted: 18 October 2023 doi:10.20944/preprints202310.1113.v1

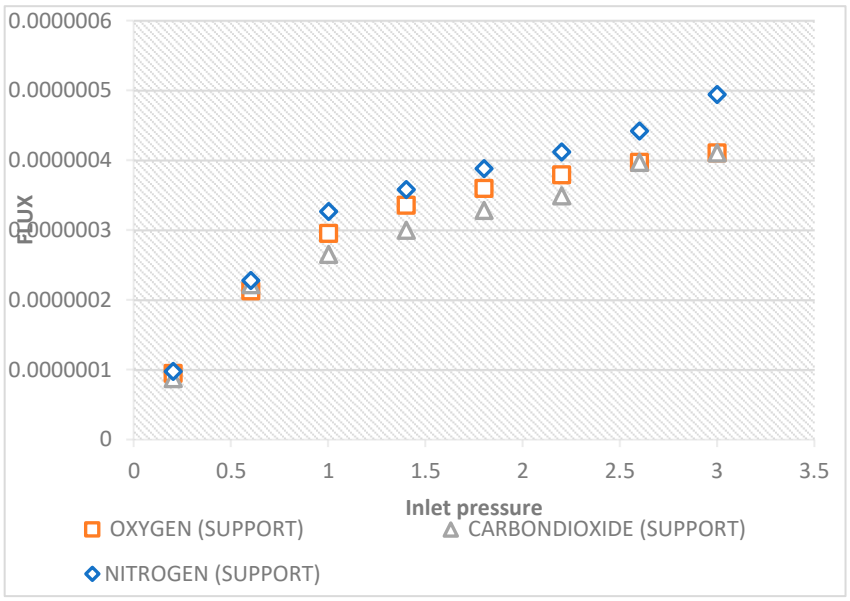

Figure 8. showing effect of flux on inlet pressure.

The effects of pressure dependence on CO_2, N_2, O_2, gas fluxes via the hydrophobic ceramic membrane support at temperatures of 20 °C are shown in the graph in Figure 8. The lowest flux was reported by O_2, which has a larger molecular weight of 32.00. Nitrogen, which has molecular weights of 28.0, reported the highest flux flowed, while CO_2, which has molecular weights of 44.0, is shown to fall between the lowest flux (O_2). As a result, it may be believed that the Knudsen type of transport mechanism is not predominant since the gas with the higher molecular weight tends to be the second flowrate. This further demonstrates the molecular weight's independence from the flow mechanism.

7.1.2. Effect of pressure dependence of CO_2, N_2, and O_2, gas permeance at 20^0c

Permeability and perm-selectivity parameters are frequently used to quantify inorganic ceramic membrane performance. Permeability is defined as the flow normalised against the pressure difference and membrane thickness (mol m. m^{-2} s 1 pa), respectively, to determine the permeability. Although the ceramic membranes' membrane thickness wasn't easily accessible, their permeance, Q (mol m^{-2} s 1 Pa^{-1}), was calculated. From the following expression, gas permeance was calculated:

$$Q = \frac{F}{A.\Delta P} \tag{2}$$

where Q is the permeance (mol m^{-2} s^{-1} pa^{-1}); F is the molar flow (mol/sec.); A is the membrane area (m^2); and P is the pressure differential (Pa) across the membrane. Effect of pressure dependence of CO_2, N_2, and O_2, gas permeance at 20^0c, is shown in Figure 9.

Preprints (www.preprints.org) | NOT PEER-REVIEWED | Posted: 18 October 2023 doi:10.20944/preprints202310.1113.v1

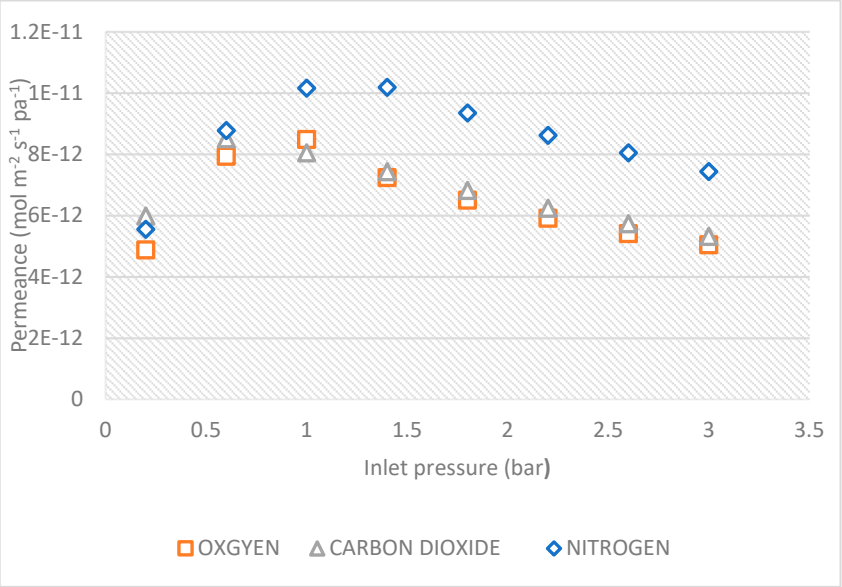

Figure 9. Effect of pressure dependence of CO_2, N_2, O_2, gas permeance at 200c.

Effect of pressure dependence of CO_2, N_2, and O_2, gas permeance at 20^{0}c, is shown in Figure 9. Nitrogen has highest permeance at a except at all pressures while from CO_2 has the lowest permeance from 0.2- 2.6, oxygen, was higher than CO_2 from 0.2 to 2.6 bar, but from 2.6- 3 bar oxygen and CO_2 had the same permeance.

According to Pandey and Chauhan 2001, who claimed that there is an inverse relationship between permeance and molecular weight, validating Knudsen flow mechanism, this phenomenon can be attributed to their respective molecular weights. Nitrogen (N_2) permeance was higher than both of CO_2 and Oxygen (O_2). As a result, only high permeance separation membranes with realistic size and pressure conditions may be considered of as a practical alternative for DAC (Fujikawa et al. 2020). In this case, there is need to modify the ceramic membrane used to increase the permeance of CO_2. Due to the modified membrane using a new flow mechanism, it is anticipated that the permeance of CO_2 will rise with membrane alteration. The Figures 3 and 7 show a flow that is consistent with Knudsen flow for an unaltered membrane at pressures greater than 0.2 bar. $CO_2 > N_2 > O_2$, the permeances of CO_2 and N_2 are also very close, their molecular weights are not. This would suggest that the flow of these gases through the barrier was accomplished by a separate flow mechanism.

7.2. Knudsen number experimental results

The results demonstrate that the direction of fluid flow affects the extent of gas permeation. The Knudsen number was plotted against inlet pressure at 20 ^{o}c, for each of the three gases. When the linear pressure gradient is considered, each plot displays the profile of the appropriate Knudsen number of the gases using a hydrophobic ceramic membrane with a pore size of 15nm. It indicates that the friction factors drop monotonically when the tangential momentum accommodation coefficient (TMAC) decreases, and the channel aspect ratio increases. Figures 3 and 8, show how the aspect ratios impact the inlet pressure in the slip-flow region. For decreasing aspect ratios, the inlet pressures are clearly higher. Inlet pressures in microchannels and nanochannels decrease as aspect ratios increase. The Knudsen regimes are contrasted with these plots (derived from Table 4) to define the gas dynamics in pores of 15nm and to study and apply the results to useful commercial applications. To define the gas dynamics at pores of 15 nm and to study and apply the findings to useful industrial applications, the Knudsen regimes are contrasted against these plots (taken from Table 4). The term “no-slip boundary condition” refers to a situation where the fluid layer is in direct contact with the wall and there is no relative movement (slip) for gases such as N_2, O_2, and CO_2 at extended inlet pressures of 0.2 to 3 bar. (see Figure 10). the value range of Kn was from 0.0 – 0.01 for

Preprints (www.preprints.org) | NOT PEER-REVIEWED | Posted: 18 October 2023 doi:10.20944/preprints202310.1113.v1

O_2. The continuum flow is assumed if the Knudsen number's normal range is 0.00 to Kn to 0.01. For N_2, Kn's value ranges from 0.01 to 0.1. The slip boundary condition is assumed in this scenario if the typical range of the Knudsen number is between 0.01 and Kn to 0.1. For CO_2, the value range of Kn is between 0.1 and 10. In this case, it is assumed that the transition flow will occur if the normal range of Knudsen numbers is 0.1 to Kn to 10.

Table 4. the gas flow characteristics based on Boltzmann's.

Knudsen number.	**0-0.01**	**0.01-0.1**	**0.1-10**	**10-100**
Flow regime	Continuum flow	Slip flow	Transistion	free molecule flow

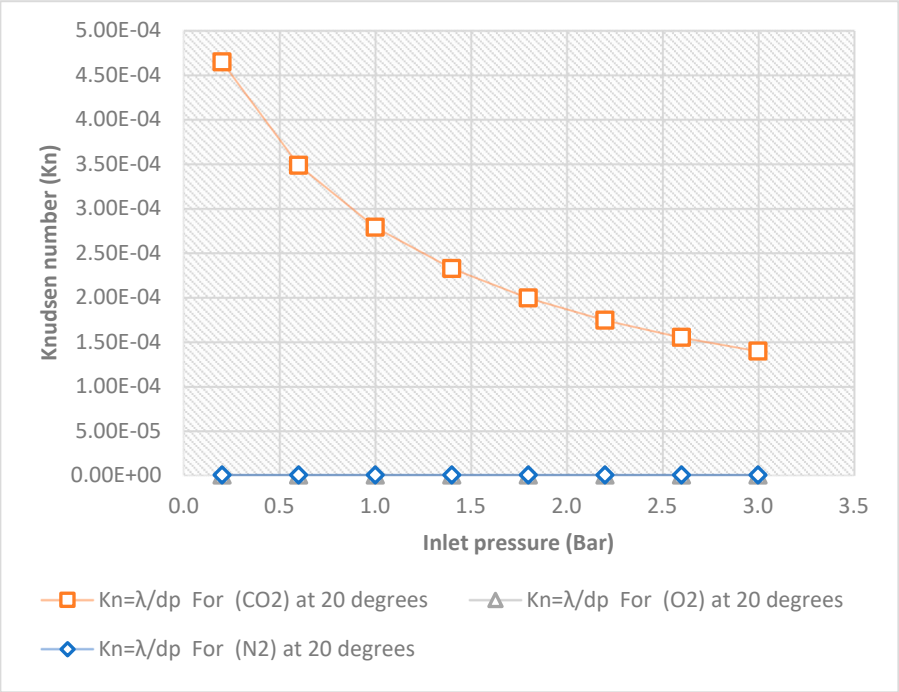

Figure 10. showing the effect of Knudsen number on inlet pressures.

7.3. Membrane snudsen selectivity of the hydrophobic ceramic membrane

Knudsen selectivity is the ration of the flow rate of different gasses as given by

$$S_{xy}=\frac{Q_Z}{Q_y} \tag{3}$$

where S_{xy} is the Knudsen selectivity of x to y; Q_x is the flow rate of x gasses; Qy is the flow rate of y gasses.

For the investigated temperature and pressure range, Tables 1 and 3 compare the experimental selectivity to the theoretical Knudsen selectivity. Equation (29) provides the theoretical selectivity of component x over y.

$$S_{x/y}=\sqrt{\frac{M_x}{M_y}} \tag{4}$$

where M_y is the molecular weight of O_2, N_2, or, and Mx is the molecular weight of the target gas, CO_2, in this case. The Knudsen selectivity attained by applying Equation (3) is relatively close to those attained by Equation (4).

Table 5 shows the theoretical and experimental selectivity of CO_2 over O_2, N_2, and at various pressures of 0.2–3 bar. According to the overall findings, the experimental Knudsen selectivity of CO_2 gas to O_2, N_2. The experimental selectivity of CO_2 selectivity to O_2 was found to be 0.92, 1.04, 0.90, 0.89, 0.91, 0.92, 1 and 1 at 0.2, 0.6, 1, 1.4, 1.8, 2.2, 2.6, and 3 bar, respectively, whereas the theoretical

Preprints (www.preprints.org) | NOT PEER-REVIEWED | Posted: 18 October 2023 doi:10.20944/preprints202310.1113.v1

Knudsen result is 1.17, making this the Knudsen result that is below theory. Table 11 displays this. Furthermore, the experimental CO_2 selectivity to N_2, was 0.89, 0.97, 0.82, 0.83, 0.85, 0.85, 0.90, and 0.83 at 0.2, 0.6, 1, 1.4, 1.8, 2.2, 2.6, and 3 bar, respectively, whereas the theoretical Knudsen selectivity is 1.25. These outcomes are below the theoretical Knudsen selectivity. This suggests that the membrane requires modification to capture CO_2 directly from the air. To further improve Knudsen selectivity, variables like pressure and membrane pore size should be decreased.

As a substitute, modifcation of membranes, which employ a molecular sieving separation mechanism, would work well as a gas separation membrane for the gases. For the separation of these gases, though, a different flow mechanism could be used. A selectivity factor of 1.2 is evidence of no separation; therefore, modifying the membrane should be geared towards achieving a selectivity higher than the theoretical selectivity because the more selective a membrane is to a particular gas, the higher the selectivity factor.

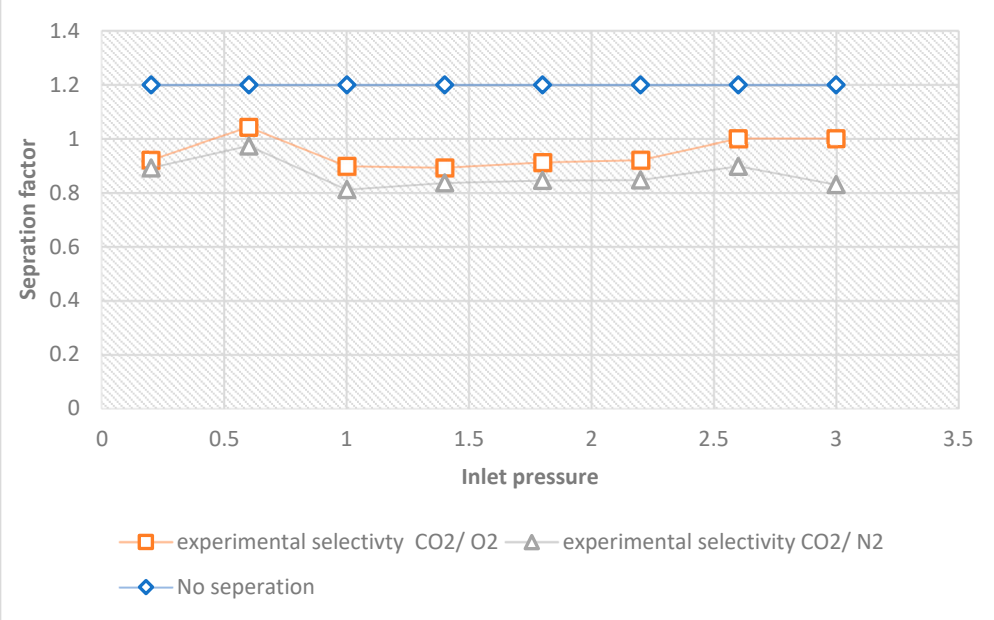

Figure 11. separation factor of hydrophobic ceramic membrane.

Table 5. Relationship between and experimental Knudsen selectivity and theoretical selectivity of 0.2-3 inlet pressure (bar).

Inlet pressure (bar).	Experimental knudsen Selectivity CO_2/O_2	experimental knudsen selectivity CO_2/N_2	Theoretical Knudsen selectivity	
0.2	0.2	0.89	CO_2/O_2	1.17
0.6	1.04	0.97	CO_2/N_2	1.25
1.00	0.90	0.82		
1.40	0.89	0.83		
1.80	0.91	0.85		
2.2	0.92	0.85		
2.6	1	0.90		
3.0	1	0.83		

8. Conclusions

Membrane technology is one of the most popular methods for collecting CO_2 because to its lower cost, easier setup and operation, and less negative environmental impact. To characterize the particles, SEM examination is used. It is clear from the SEM study that the particles are distributed uniformly across the ceramic membrane's whole surface. The particles are evenly distributed throughout the

entire surface of the hydrophobic ceramic membrane. Notably, the hydrophobic ceramic membrane has a smooth and faultless surface with no fractures. The s alumina support's elemental compositions were ascertained using energy dispersive X-ray analysis (EDAX). The observation from contact angle measurements indicates an occurrence of adsorption, suggesting that interactions were taking place. Based on the outcomes, it can be deduced that the ceramic membranes used possess hydrophobic properties. The experimental contact angle results, employed as a characterization technique, validated the distinctions in the surface's physicochemical attributes. Interpretation of these results suggests that the ceramic membrane's surface free energy indicates relatively lower interactions with water. This outcome indicates a low surface free energy for the sample, signifying limited interaction with the liquid.

At temperatures of 20^0 c, the effect of pressure dependency on CO_2, N_2, and O_2 gas fluxes through the ceramic membrane support was investigated. The lowest flux was reported by O_2, which has a larger molecular weight of 32.00. Nitrogen, which has molecular weights of 28.0, reported the highest flux flowed, while CO_2, which has molecular weights of 44.0, is shown to fall between the lowest flux (O_2). At a temperature of $20^{0°}$C, the effect of pressure dependence on CO_2, N_2, and O_2 gas permeance was examined. According to the findings, Nitrogen has highest permeance at a except at all pressures while from CO_2 has the lowest permeance from 0.2- 2.6, oxygen, was higher than CO_2 from 0.2 to 2.6 bar, but from 2.6- 3 bar oxygen and CO_2 had the same permeance. To increase the permeance of CO_2, it is necessary in this situation to modify the ceramic membrane. By analyzing the gas flow using the Knudsen Number, the results demonstrate that the direction of fluid flow affects the degree of penetration of the pertinent gases. Investigated were both the experimental and theoretical Knudsen selectivity. It might be said that the results are practically attainable. This shows that to directly capture CO_2 from N_2 and O_2, the membrane needs to be modified. Variables like temperature and membrane pore size should be reduced to further increase Knudsen selectivity.

Author Contributions: For research articles with several authors, a short paragraph specifying their individual contributions must be provided. The following statements should be used "Conceptualization, Idris Hashim. and Habiba methodology, Idris Hashim formal analysis, Idris Hashim. Investigation, Idris Hashim. Resources, Habiba.; writing—original draft preparation, Idris Hashim writing—review and editing , Muktar Ramalan, and Flurence Aisueni and Priscilla Ogunlude visualization, Ayo Giwa and James Njuguna supervision, Mamdud hossain and Aditiya funding acquisition, Habiba and Ayo Giwa

Funding: In addition, we warmly acknowledge the sponsorship from Petroleum Trust and development Fund, Nigeria. And McAlpha, Canada for their support.

Acknowledgments: Sincere appreciation is extended by the author to the School of Life Sciences at Robert Gordon University for providing the SEM and EDXA observations as well as to the Centre for Process Integration and Membrane Technology of Robert Gordon University for providing the fresh membrane used in the study. In addition, we warmly acknowledge the sponsorship from Petroleum Trust and development Fund, Nigeria. And McAlpha, Canada for their support.

Conflicts of Interest: Declare conflicts of interest or state "The authors declare no conflict of interest."

References

1. Bounaceur, R., Lape, N., Roizard, D., Vallieres, C. and Favre, E., 2006. Membrane processes for post-combustion carbon dioxide capture: a parametric study. *Energy*, *31*(14), pp.2556-2570.
2. FREUND, P., 2013. Anthropogenic climate change and the role of CO2 capture and storage (CCS). *Geological Storage of Carbon Dioxide (CO2).* Elsevier. pp. 3-25
3. FUJIKAWA, S., SELYANCHYN, R. and KUNITAKE, T., 2021. A new strategy for membrane-based direct air capture. *Polymer Journal*, 53(1), pp. 111-119
4. HANSEN, J. et al., 2010. Global surface temperature change. Rev. Geophys., 48, RG4004.
5. HASHIM, I.A. et al., 2022. Characterization of membranes for advanced direct carbon capture.
6. KEITH, D.W. et al., 2018. A process for capturing CO2 from the atmosphere. *Joule*, 2(8), pp. 1573-1594
7. Kumar, S., Dang, T.D., Arnold, F.E., Bhattacharyya, A.R., Min, B.G., Zhang, X., Vaia, R.A., Park, C., Adams, W.W., Hauge, R.H. and Smalley, R.E., 2002. Synthesis, structure, and properties of PBO/SWNT Composites&. *Macromolecules*, *35*(24), pp.9039-9043.
8. LIANG, C. et al., 2012. A comparison on gas separation between PES (polyethersulfone)/MMT (Na-montmorillonite) and PES/TiO2 mixed matrix membranes. *Separation and Purification Technology*, 92, pp. 57-63.

9. MAXIMILLIAN, J. et al., 2019. Pollution and environmental perturbations in the global system. *Environmental and pollution science.* Elsevier. pp. 457-476
10. SANZ-PEREZ, E.S. et al., 2016. Direct capture of CO2 from ambient air. *Chemical reviews,* 116(19), pp. 11840-11876
11. XIA, J. et al., 2011. Liquidlike poly (ethylene glycol) supported in the organic–inorganic matrix for CO2 removal. *Macromolecules,* 44(13), pp. 5268-5280.
12. YU, X. et al., 2015. CO2 capture using a superhydrophobic ceramic membrane contactor. *Journal of Membrane Science,* 496, pp. 1-12.
13. Zou, L., Liu, Y., Wang, Y. and Hu, X., 2020. Assessment and analysis of agricultural non-point source pollution loads in China: 1978–2017. *Journal of Environmental Management*, *263*, p.110400.